Liquid Crystals
Publication details, including instructions for authors and subscription information:
http://www.informaworld.com/smpp/title~content=t713926090

Bold relief fabrication by means of electroconvection: basic properties of a suitable mixture

M. A. Zöller[a]; N. Stich[a]; S. A. Benning[a]; A. Hoischen[a]; H. -S. Kitzerow[a]
[a] Department of Chemistry, Faculty of Science, University of Paderborn, Paderborn, Germany

Online publication date: 23 April 2010

To cite this Article Zöller, M. A. , Stich, N. , Benning, S. A. , Hoischen, A. and Kitzerow, H. -S.(2010) 'Bold relief fabrication by means of electroconvection: basic properties of a suitable mixture', Liquid Crystals, 37: 4, 383 — 388
To link to this Article: DOI: 10.1080/02678291003632603
URL: http://dx.doi.org/10.1080/02678291003632603

Liquid Crystals,
Vol. 37, No. 4, April 2010, 383–388

Taylor & Francis
Taylor & Francis Group

Bold relief fabrication by means of electroconvection: basic properties of a suitable mixture

M.A. Zöller, N. Stich, S.A. Benning, A. Hoischen and H.-S. Kitzerow*

Department of Chemistry, Faculty of Science, University of Paderborn, Warburger Str. 100, D-33098 Paderborn, Germany

(Received 30 September 2009; final version received 18 January 2010)

Electroconvection of liquid crystals does not only lead to a large variety of spontaneously formed patterns, but these patterns can also be used as a template for the fabrication of polymer surfaces exhibiting a periodic bold relief. Here, a useful room-temperature nematic mixture consisting of two photostable liquid crystals and a photosensitive cross-linker is presented. Its stability diagram in the frequency-voltage plane, the influence of monomer concentration and the topography of the resulting polymer surfaces are described.

Keywords: electroconvection; liquid crystals; photopolymerisation; micro- and nanostructures

1. Introduction

The electric field-induced formation of periodic convection rolls (Williams domains) [1] and the electro-optic application of the transition from a stable, uniformly aligned transparent state to a highly scattered convective state (dynamic scattering mode) [2] are among the longest and most extensively studied field effects in liquid crystals [3, 4]. Nevertheless, pattern formation in liquid crystals [5] is an ongoing subject of modern research. The standard model by Carr–Helfrich [6–8], which describes the behaviour of a uniformly planar-oriented nematic liquid crystal with negative dielectric anisotropy $\Delta\varepsilon$ and positive anisotropy $\Delta\sigma$ of the electric conductivity [($\Delta\varepsilon < 0$, $\Delta\sigma > 0$, parallel anchoring):= '(–, +, ||)'], was also shown to explain the possibility of pattern formation in nematic liquid crystals with $\Delta\varepsilon > 0$, $\Delta\sigma < 0$ and perpendicular (homeotropic) anchoring (+, –, ⊥) [9–12]. Electroconvection, however, was also observed in many non-standard cases, e.g. (–, –, ||) [12–13], (+, +, ||) [14] or (–, +, ⊥) ⇒ 'prewavy pattern' [15–18]. Most recently, the influence of flexo-electric contributions on the pattern formation was studied [13].

Since the 1980s, in-situ photopolymerisation of reactive liquid crystals has been extensively studied and considered for fabricating optical memories, compensators, filters, mirrors, liquid crystal displays and organic light-emitting diodes [19]. Complex polymer networks can be formed if mixtures of photoreactive and non-reactive liquid crystals are exposed to UV radiation [20–22]. In previous papers [23–25], we reported that such complex polymer structures can not only be formed under equilibrium conditions, but also under the non-equilibrium conditions of electroconvection. The photoreaction then leads to a polymer structure that resembles the pattern that was present during the polymer formation. Unlike the dissipative structure that was present during the photoreaction, the pattern imprinted in the resulting polymer is permanently fixed. It was shown that the non-reactive components can be separated and the procedure can be repeated, thereby leading to a superposition of different patterns [24]. Under appropriate conditions, the lattice constant of the periodic structure, which is typically of the order of the sample thickness and thus larger than a few micrometres, can be reduced down to the submicrometre range [25]. Unfortunately, most of the mixtures studied earlier were difficult to handle. They either exhibited a melting point above room temperature and thus required careful temperature control, or contained 'non-reactive' components with limited photostability, or consisted of many compounds with different functionality, including chiral additives. The present paper describes a suitable non-chiral mixture, which is nematic at room temperature and easy to handle. It is based on the eutectic mixture of just two photostable nematic compounds, contains variable concentrations of one liquid-crystalline diacrylate as a cross-linkable monomer, and a small amount of photo-initiator. We describe its stability diagram and the basic properties of polymer films formed under different conditions.

2. Experiments

The mixture studied is based on the eutectic (2:1) mixture of two nematic esters (Table 1), 4-methoxy-(4-pentyl-phenyl)-benzoate (ME 10.5, Merck) and 4-hexyloxy-(4-pentyl-phenyl)-benzoate (ME 60.5) (Merck). To this mixture, 5–25 weight percentage of the reactive nematic liquid crystal 1,4-bis[3-(acryloyloxy)propyloxy]-2-methyl benzene (RM 257) (Merck) was added as a cross-linkable, photoreactive

*Corresponding author. Email: Heinz.Kitzerow@upb.de

ISSN 0267-8292 print/ISSN 1366-5855 online

DOI: 10.1080/02678291003632603
http://www.informaworld.com

Table 1. Structures of the compounds used.

ME 10.5

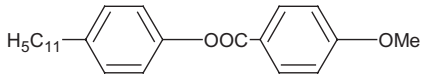

ME 60.5

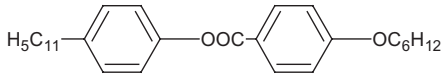

RM 257

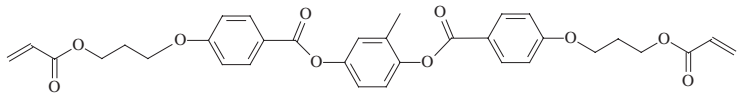

I 651

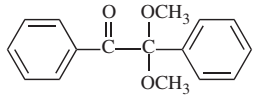

Table 2. Composition of the samples investigated.

Tag of the sample	Mass fractions (%)				Clearing temperature (°C)
	ME 10.5	ME 60.5	RM 257	I 651	
ET5	62.6	31.4	5	1	48.9
ET10	59.4	29.6	10	1	52.5
ET15	56	28	15	1	56.6
ET25	49.3	24.7	25	1	62.5
ET50	32.7	16.3	50	1	84.8
ET75	16.0	8.0	75	1	101.1

compound (Table 2). For completeness, the clearing temperatures of mixtures containing 50 and 75 weight percentage of RM257 are also given in Table 2. However, these mixtures crystallise at temperatures above room temperature. In order to polymerise the system, 1 weight percentage of the photo-initiator Irgacure 651 (Ciba Geigy) was added to some of the mixtures.

In order to apply electric fields, the nematic liquid crystal mixtures were filled in glass cells with transparent indium tin oxide (ITO) electrodes. Both commercial cells (EHC, Hogashik, Japan) and self-fabricated cells were used. The commercial cells exhibited a cell gap d of 6, 10 and 15 μm. Their inner surfaces were coated with a polyimide alignment layer that is rubbed to provide a parallel alignment of the director in the plane of the surface. In addition, cells were fabricated with a cell gap of 11 μm in our laboratory. The inner surfaces of the self-made cells were coated with transparent ITO and equipped with a photo-alignment layer. For the latter purpose, the monomer LPP JP 265 CP (Rolic Ltd, Allschwil, Switzerland) was deposited by spin-coating and photopolymerised with polarised UV radiation to form an anisotropic alignment layer (the easy axis of liquid crystal anchoring on the surface was perpendicular to the UV plane of polarisation). The cells were filled with the liquid crystal mixture by capillary forces. Subsequently, electric contacts were soldered on to the ITO.

In order to induce William domains and other dissipative structures, a sine wave voltage ($f = 10$–800 Hz, $V_{\text{pk-pk}} = 8$–200 V) was applied. The stability and induced patterns depend strongly on frequency and voltage. The respective stability diagrams are described below. Cells containing the photo-initiator were then photopolymerised under the influence of an electric field. Two different UV sources were used for this purpose. A quartz-halogen lamp (Opticure, Norland Products, Cranbury, NJ, USA) was used for small intensities (<10 mW cm^{-2}), and a mercury-arc lamp (Bluepoint 4, Hönle UV Technology, Gräfelfing, Germany) for high intensities (100–10,000 mW cm^{-2}). The transmission of the substrates that cover the liquid crystal exceeded 70% in the UV-A spectral region. After complete polymerisation (0.5 to 1 min, depending on UV intensity), the voltage was switched off.

3. Results

As expected, the samples investigated showed a nematic phase at room temperature. The clearing temperature increased with increasing concentration of the reactive monomer RM 257 (Table 2). Due to negative dielectric anisotropy and positive anisotropy of the conductivity, the application of AC voltages to the samples with uniform parallel anchoring of the director lead to the formation of convection rolls above a critical voltage, which depended strongly on the frequency of the AC field. Normal rolls were observed close to the onset of convection for low frequencies (conducting regime), while a chevron pattern appeared at high frequencies (dielectric regime). The stability diagram in the frequency-voltage plane (Figure 1) indicated a strong increase in critical voltage with increasing frequency in the range below the

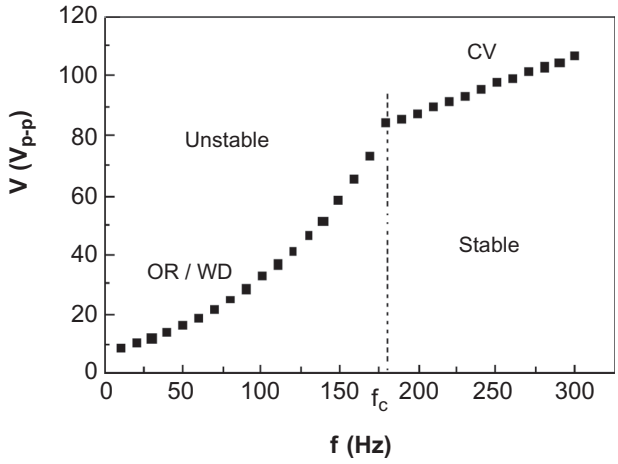

Figure 1. Stability diagram of the mixture ET5. CV, chevron pattern; OR, oblique rolls; WD, Williams domains.

critical frequency f_c (around 180 Hz for the mixture ET5), and a rather moderate increase in critical voltage with increasing frequency in the range above the critical frequency. This behaviour is in agreement with other liquid crystals that exhibit $\Delta\varepsilon < 0$ and $\Delta\sigma > 0$ and corresponds to the typical behaviour described by the standard model [6–8].

The critical frequency f_c, which separates the dielectric from the conductive regime, was found to decrease with an increasing amount of reactive monomer (Figure 2). This indicates that the monomer RM 257 shows a lower conductivity than the mixture of esters ME 10.5 and ME 60.5, since the critical frequency f_c is known to increase linearly with increasing conductivity [3].

In order to study the influence of the cell gap on electroconvection, self-made cells with a thickness of 11 μm were studied in addition to commercial cells (EHC) with $d = 6$, 10 and 15 μm. At a given frequency, the onset voltage for the formation of normal rolls (Williams domains) remained constant, if the sample

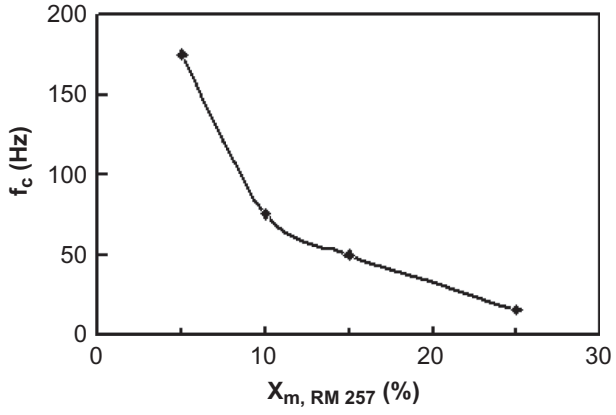

Figure 2. Critical frequency f_c versus mass fraction of the reactive monomer RM257.

thickness was varied between 6 and 15 μm (Figure 3). This is in agreement with the expectation from the standard model that this voltage is independent of sample thickness [3]. However, the onset voltage for the formation of the chevron pattern in the dielectric regime increased continuously with increasing cell gap. Dividing the critical voltages in the dielectric regime by the respective cell gap indicated that critical field strength is more appropriate than the voltage in order to describe the stability diagram in the dielectric regime. Again, this is expected from the standard model [3]. However, careful inspection showed that the onset did not increase linearly with cell gap d, so that the field strength seemed to decrease slightly with increasing d (Figure 3). In addition, the critical frequency of our samples with different thicknesses varied slightly. We speculate that the latter effect, which is not expected by the Carr–Helfrich model, might be attributed to different anchoring conditions in our self-made cells.

If an AC voltage is applied and thus a pattern induced, this pattern can usually be fixed due to photopolymerisation by exposing the sample to UV radiation. If so, the pattern remains stable when the voltage is removed after polymerisation. However, it is interesting to note that sometimes the pattern disappeared or was replaced by a different pattern during exposure. An example is illustrated in Figure 4, which shows pictures taken by polarising microscopy for a cell containing 5 weight percentage RM 257 and 1 weight percentage of the photo-initiator before and after photopolymerisation. Prior to exposure, the sample showed parallel stripes perpendicular to the director (normal rolls) at a voltage of 10.6 V with a frequency of 10 Hz (Figure 4(a)). However, the pattern changed during the photopolymerisation and a square pattern formed during the first seconds of the polymerisation process (Figure 4(b)). This phenomenon can be attributed to the increasing viscosity of the mixture during polymerisation, since the viscosity is known to affect the stability diagram considerably. After purifying the sample from non-reactive residuals, the remaining polymer showed both regions with parallel stripes and the grid pattern. The grid pattern represented in Figure 4(b) resembles the grid pattern that was extensively described earlier [26].

After purification, the two glass substrates of the cell were separated and the surface of the polymer investigated by means of atomic force microscopy (AFM). The surface topography seen in AFM images (Figure 5) revealed a hierarchical structure of the polymer network with several characteristic length scales. Images with low resolution showed a topography that resembles the dissipative structure that was present during the polymerisation process. For example, Figure 5(a) shows vertical stripes, which correspond

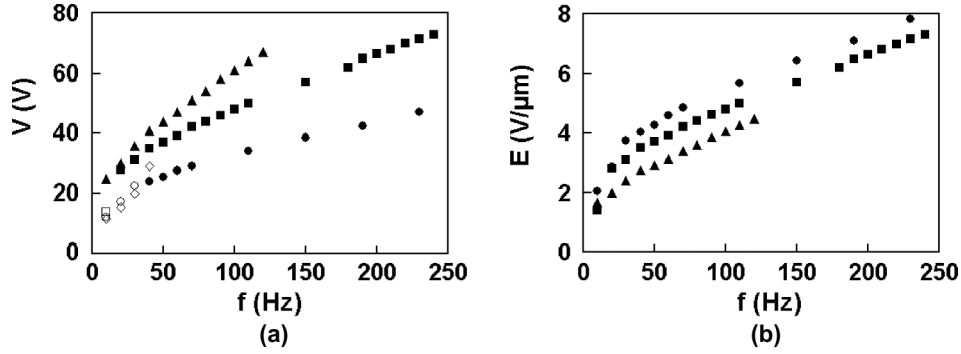

Figure 3. (a) Critical voltage and (b) critical field strength versus frequency for different cell thicknesses (● = 6 µm, ■=10 µm, ◆=11 µm and ▲=15 µm).

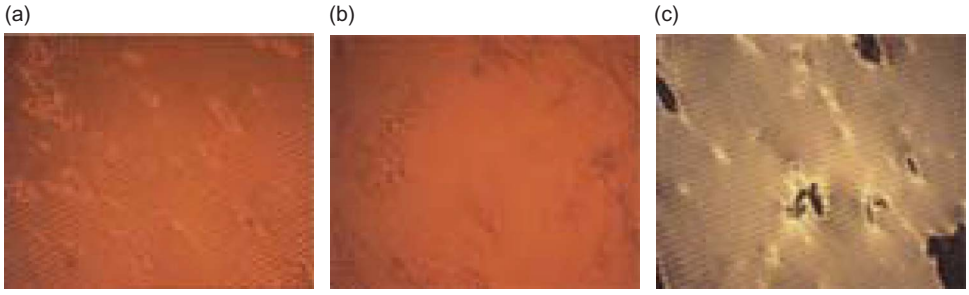

Figure 4. Polarising microscopy pictures of the polymer films: (a) before photopolymerisation; (b) after photopolymerisation; (c) after the non-reactive components have been removed. The cell was filled with ET10 and polymerised under a field with a frequency of 20 Hz and a peak-to-peak voltage of 10.3 V.

to former Williams domains. Some additional lines in a transverse direction can be seen in the lower left corner. They indicate the partial transition to the square grid pattern. The lines corresponding to Williams domains have a distance of 22 µm and a maximum height of 800 nm. A more detailed view of the intersections of the vertical and horizontal lines is shown in Figure 5(b). The distance between two transverse lines is 18 µm (slightly smaller than the distance between the vertical lines). The height profile of the grid pattern is more pronounced in comparison to the parallel stripes. For the grid pattern, the height differences reach an amplitude of 1.5 µm.

Images with high resolution, such as Figure 5(c), show that the polymer network has a porous structure. It consists of filaments that are aligned along the rubbing direction of the alignment layer. The polymer fibres have a width of 100–180 nm. A cross-section of the polymer surface (Figure 6) shows height variations of this order of magnitude of around 100 nm and

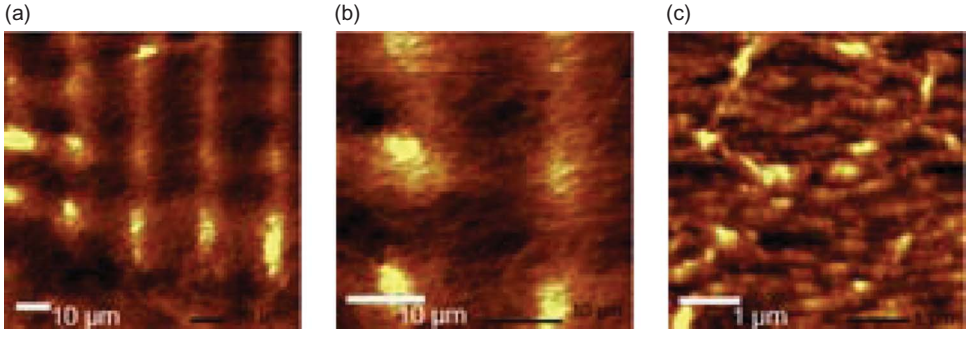

Figure 5. Atomic force microscopy images of the polymer surface obtained from the sample ET5 at different magnifications: (a) 95 µm × 95 µm; (b) 40 µm × 40 µm; (c) 5 µm × 5 µm.

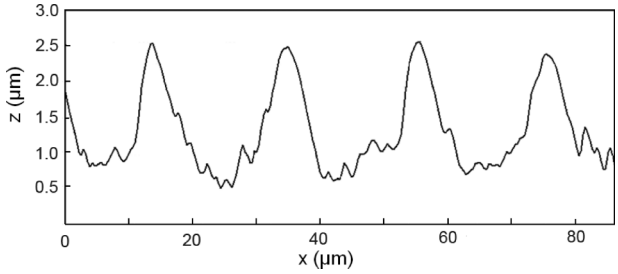

Figure 6. Cross-section of the surface topography (height z versus lateral position x) for the same sample as shown in Figure 5.

the coarse height variations with an amplitude in the order of around 1 μm.

With respect to the discussion of possible mechanisms (section 4), it is interesting to note that the polymer surfaces of the films attached to the two substrates of the sample may differ with respect to both the quality of the pattern and the amplitude of the surface modulation. These differences cannot be explained only by the absorption of UV radiation within the liquid crystal. In fact, the transmission of the liquid crystal layer was found to be rather large (almost 90% in the UV-A region). In addition, the surface topography sometimes did not resemble precisely the simple convection rolls that were present during polymerisation, but show additional features. For example, the AFM image presented in Figure 7 shows double peaks rather than a simple sinusoidal surface variation. It can be concluded that the spatial refractive index

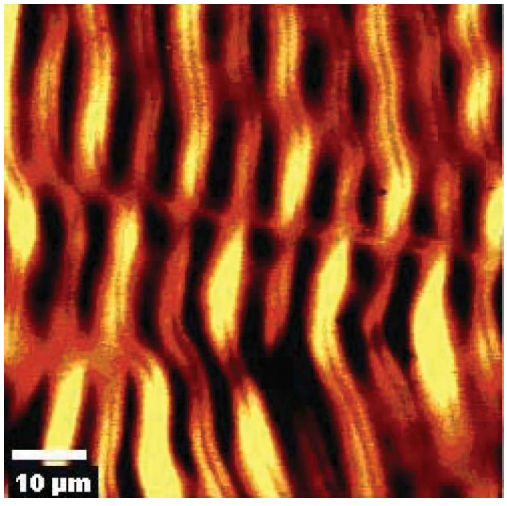

Figure 7. Atomic force microscopy image of the surface topography for a sample obtained from the mixture ET25, polymerised under the influence of an AC voltage (8 Hz, 15 V) using UV-A radiation with an intensity of 100 mW cm^{-2}. The height variation between dark and bright positions corresponds here to 120–130 nm.

variation due to electroconvection has a focusing or defocusing effect, thereby leading to a non-uniform UV intensity distribution, which in turn affects the local polymerisation rate.

4. Summary

In conclusion, we found and characterised a suitable mixture that showed similar surface variations of the polymer structure formed under non-equilibrium conditions as reported previously [23–25]. The mixtures simply contained two photochemically very stable compounds and a photoreactive mesogenic cross-linker. They exhibited a nematic phase at room temperature and showed the typical properties of electroconvection described by the Carr–Helfrich mechanism (Figure 1). The critical frequencies were surprisingly low and even decreased with increasing concentration of the cross-linker (Figure 2). An influence of the flexoelectric effect, which was detected for higher homologues of the esters ME 10.5 and ME 60.5, cannot be excluded. Variation of the sample thickness indicated that the critical voltage for onset of instabilities was independent of sample thickness in the conducting regime, while the critical voltage increased with sample thickness in the dielectric regime (Figure 3). Again, this is in qualitative agreement with the Carr–Helfrich model, where the onset of instabilities is appropriately described by a characteristic voltage in the conducting regime, and characteristic field strength in the dielectric regime, respectively. Surprisingly, the values of the critical frequency seemed to vary in the samples with different thicknesses. However, we cannot exclude that this variation was due to different anchoring conditions. Thorough investigations under different polymerisation conditions indicated that the pattern may change during photopolymerisation (Figure 4). This observation is reasonable since both the viscosity and local compositions change while the polymerisation is proceeding. The surfaces of the resulting polymer films showed both a coarse structure and a fine structure (Figure 5). The maximum amplitude of the surface variation was 1.5 μm (Figure 6).

The results obtained so far are not sufficient for conclusive knowledge about the precise mechanism that leads to the surface patterning of the resulting polymer. However, it is interesting to note that the polymer films formed at the front substrate may differ from those attached to the back substrate, in spite of the relatively large transmission of the liquid crystal. This seems to indicate that the focusing effect of the patterns induced by electroconvection has a major influence on the local UV intensity and thus on the local polymerisation speed. Indeed, the observation of

double peaks (Figure 7) very much resembles the intensity distributions that appear in different planes of electroconvective samples due to the focusing effect [27]. More detailed studies on the precise mechanism are under consideration.

Acknowledgements

The authors would like to thank Yoshiki Hidaka for illuminating discussions. Financial support by the Deutsche Forschungsgemeinschaft (project KI 411/5-2) is gratefully acknowledged.

References

[1] Williams, R. *J. Chem. Phys.* **1963**, *39*, 384–388.
[2] Heilmeier, G.H.; Zanoni, L.A.; Barton, L.A. *Appl. Phys. Lett.* **1968**, *13*, 46–47.
[3] de Gennes, P.G.; Prost, J. *The Physics of Liquid Crystals*, 2nd edition; Clarendon: Oxford, 1992.
[4] Chandrasekhar, S. *Liquid Crystals*, 2nd edition; Cambridge University Press: Cambridge, 1992.
[5] Buka, A.; Kramer, L., Eds.; *Pattern Formation in Liquid Crystals*; Springer-Verlag: New York, 1996.
[6] Carr, E.F. *Mol. Cryst. Liq. Cryst.* **1969**, *7*, 253–268.
[7] Helfrich, W. *J. Chem. Phys.* **1969**, *51*, 4092.
[8] Bodenschatz, E.; Zimmermann, W.; Kramer, L. *J. Physique* **1988**, *49*, 1875–1899.
[9] Buka, Á.; Dressel, B.; Otowski, W.; Camara, K.; Toth-Katona, T.; Kramer, L.; Lindau, J.; Pelzl, G.; Pesch, W. *Phys. Rev. E: Stat., Nonlinear, Soft Matter Phys.* **2002**, *66*, 051713.
[10] Buka, Á.; Dressel, B.; Kramer, L.; Pesch, W. *Phys. Rev. Lett.* **2004**, *93*, 044502.
[11] Buka, Á.; Dressel, B.; Kramer, L.; Pesch, W. *Chaos* **2004**, *14*, 793–802.
[12] Kochowska, E.; Németh, S.; Pelzl, G.; Buka, Á. *Phys. Rev. E: Stat., Nonlinear, Soft Matter Phys.* **2004**, *70*, 011711.
[13] Krekhov, A.; Pesch, W.; Éber, N.; Tóth-Katona, T.; Buka, Á. *Phys. Rev. E: Stat., Nonlinear, Soft Matter Phys.* **2008**, *77*, 021705.
[14] Dressel, B.; Pesch, W. *Phys. Rev. E: Stat., Nonlinear, Soft Matter Phys*, **2003**, *67*, 031707.
[15] Huh, J.-H.; Hidaka, Y.; Rossberg, A.G.; Kai, S. *Phys. Rev. E: Stat., Nonlinear, Soft Matter Phys.* **2000**, *61*, 2769–2776.
[16] Huh, J.-H.; Hidaka, Y.; Yusuf, Y.; Éber, N.; Tóth-Katona, T.; Buka, Á.; Kai, S. *Mol. Cryst. Liq. Cryst.* **2001**, *364*, 111–122.
[17] Huh, J.-H.; Yusuf, Y.; Hidaka, Y.; Kai, S. *Phys. Rev. E: Stat., Nonlinear, Soft Matter Phys.* **2002**, *66*, 031705.
[18] Éber, N.; Buka, Á. *Phase Transitions* **2005**, *78*, 433–442.
[19] Kelly, S.M. *Flat Panel Displays: Advanced Organic Materials*; Royal Society of Chemistry: Cambridge, 2000.
[20] Broer, D.J.; Van Haaren, J.A.M.M.; Lub, J. *SPIE–Int. Soc. Opt. Eng. Proceedings* **2000**, *4107*, 59–68.
[21] Hikmet, R.A.M. *Liq. Cryst.* **2006**, *33*, 1407–1418.
[22] Crawford, G.P.; Zumer, S., Eds.; *Liquid Crystals in Complex Geometries Formed by Polymer and Porous Networks*; Taylor & Francis: London, 1996.
[23] Miessen, N.; Glossmann, J.; Hoischen, A.; Kürschner, K.; Kitzerow, H. *ChemPhysChem* **2001**, *11*, 691–694.
[24] Stich, N.; Kitzerow, H.-S. *J. Appl. Phys.* **2005**, *97*, 033519.
[25] Hoischen, A.; Benning, S.; Kitzerow, H.-S. *Appl. Phys. Lett.* **2008**, *93*, 131903.
[26] Kai, S.; Yamaguchi, K.; Hirakawa, K. *Jpn. J. Appl. Phys.* **1975**, *14*, 1385–1386.
[27] Kondo, K.; Arakawa, M.; Fukuda, A.; Kuze, E. *Jpn. J. Appl. Phys.* **1983**, *22*, 394–399.